Theory of Methane Dehydrogenation on Pt{110}(1 × 2). Part II: Microscopic Reaction Pathways for $CH_x \rightarrow CH_{x-1}$ ($x = 1-3$)

M. A. Petersen, S. J. Jenkins, and D. A. King*

Department of Chemistry, University of Cambridge, Lensfield Road, Cambridge CB2 1EW, United Kingdom

Received: December 16, 2003

Microscopic reaction pathways for the transformation of chemisorbed methyl to atomic carbon on Pt{110}-(1 × 2) have been identified using calculations based on density functional theory in combination with a constrained minimization technique. For CH_3 and CH_2 dehydrogenation, calculated activation energies of 0.34 eV (33 kJ mol^{-1}) and 0.56 eV (54 kJ mol^{-1}) are obtained, respectively. For CH dehydrogenation, the calculated activation barrier of 1.20 eV (116 kJ mol^{-1}) is in excellent agreement with the experimentally determined barrier of 1.25 eV (121 ± 3 kJ mol^{-1}).[1] The resulting calculated reaction-energy profile for the conversion of CH_3 to CH and ultimately carbon on Pt{110}(1 × 2) is reported and discussed in terms of previous experimental results obtained for this system.

I. Introduction

The catalytic partial oxidation of methane to synthesis gas (syngas, a mixture of CO and H_2, ideally in a 1:2 ratio) has been successfully demonstrated over Pt{110}(1 × 2) using molecular beam techniques.[2] To fully elucidate the reaction mechanism that governs the production of synthesis gas on this surface, it is beneficial to begin by characterizing the initial processes of methane dissociative adsorption and decomposition on Pt{110}(1 × 2). To this end, detailed studies of the dissociative sticking probability as a function of surface temperature, adsorbate coverage, and molecular translational and vibrational energy have been conducted.[3−5] Furthermore, Watson and co-workers were successfully able to identify the stable products of methane dissociative adsorption on Pt{110}(1 × 2) as a function of surface temperature.[6] Methylidyne (CH) was found to be the stable product in the surface-temperature range of 300−450 K and was found to decompose to atomic carbon and gaseous H_2 on heating the surface above 470 K. In addition, an activation energy of 121 ± 3 kJ mol^{-1} for methylidyne dehydrogenation was obtained using temperature-programmed reaction spectroscopy (TPRS).[1]

Hydrogen−deuterium exchange experiments[7] further established that methylidyne can be deuterated to gaseous methane, whereas carbon that is formed as a result of methylidyne decomposition is stable to deuteration over the surface-temperature range of 250−700 K. The results for CH deuteration were found to be consistent with a stepwise deuteration mechanism, with more than 95% of the surface methylidyne being removed by deuteration. From a kinetic analysis of the results of the hydrogen−deuterium exchange experiments, activation barriers of 70 and 73 kJ mol^{-1} were estimated for the forward and reverse surface reactions of deuterium exchange in methylidyne (i.e., $CH_a + D_a \rightleftharpoons CD_a + H_a$). This latter result provides a basis of comparison for the ab initio determination of the activation barrier for the surface hydrogenation of methylidyne to methylene (CH_2).

The decomposition of methane to carbon has been investigated on a number of transition-metal surfaces using first principles calculations in which the transition-state geometry and corresponding activation energy have been obtained for each sequential dehydrogenation reaction. This has been achieved on Ni{111},[8,9] Ru{0001},[10] Ru{1120},[11] Pt{111},[12−14] Cu{111},[12,13,15] and Pd{100}.[16] The nature of the transition states accessed in the de/hydrogenation reactions has been discussed extensively by Michaelides and Hu,[13,14] in particular, with regard to elementary hydrogenation reactions on close-packed transition-metal surfaces. For the Pt{111} surface, the dissociating hydrogen atom was preferentially located near an atop position in the transition-state geometry, with the "heavier" fragment located close to a site determined by the valency of the fragment. Liu and Hu[17] have performed a detailed analysis of the origin of the energy barrier for elementary hydrogenation reactions on transition-metal surfaces and have recently extended their discussion to include elementary catalytic reactions on stepped and stepped-kinked surfaces.[18]

Furthermore, with regard to their involvement in the surface decomposition of methane, CH_x ($x = 0-3$) fragments are also thought to play a role in a number of catalytic processes of industrial interest,[19,20] notably, the Fischer−Tropsch synthesis reaction[20−24] in which long-chain hydrocarbons are generated from synthesis gas. This has led to a number of recent theoretical studies in which the mechanism of the Fischer−Tropsch reaction has been addressed[25−27] and in which the importance of C_1 hydrocarbon fragments, in particular, CH, has been demonstrated.

In this paper, we extend the results of our previous study[28] in which the chemisorption of CH_x ($x = 3-0$) species on Pt{110}(1 × 2) has been examined in detail. In the current work, we identify microscopic reaction pathways and corresponding transition-state structures that characterize the sequential decomposition of adsorbed methyl (CH_3) to atomic carbon on the missing-row reconstructed Pt{110}(1 × 2) surface. The calculations serve to supplement and extend the experimental results obtained for this system using molecular beam techniques, together yielding a detailed understanding of the process of methane decomposition on Pt{110}(1 × 2).

* Corresponding author. E-mail: dak10@cam.ac.uk.

10.1021/jp037881r CCC: $27.50
Published on Web 04/15/2004

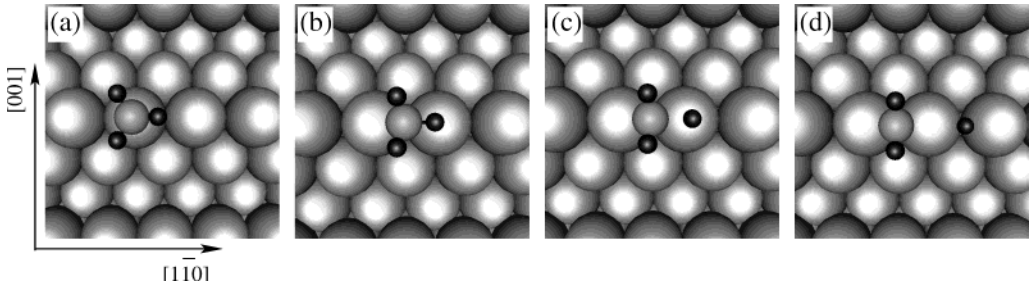

Figure 1. Methyl dehydrogenation reaction pathway on Pt{110}(1 × 2). (a) Initial state, (b) local minimum with the CH_3 moiety displaced and tilted toward the bridge site, (c) transition state, and (d) final state with coadsorbed nascent CH_2 and H. Large gray spheres represent Pt atoms, small gray spheres indicate carbon atoms, and black spheres denote hydrogen atoms.

II. Calculation Methodology

Total-energy pseudopotential calculations were performed within the framework of density functional theory (DFT), as implemented in the CASTEP code.[29] The electronic wave functions were expanded in terms of a basis set of plane waves up to a kinetic energy cutoff of 310 eV. The exchange-correlation energy was described using the Perdew−Wang (PW91) form[30] of the generalized gradient approximation (GGA). Electron−ion interactions were described by ultrasoft pseudopotentials[31] on Pt, C, and H. A total of 10, 1, and 4 valence electrons for each Pt, H, and C atom, respectively, were thus explicitly treated in the calculations.

The calculations were performed within a supercell of length equivalent to 14 layers of Pt in the surface normal direction. A six-layer slab was used to represent the Pt{110} surface within a (2 × 2) surface unit cell. The vacuum region between the slabs was thus equivalent to eight layers of Pt, ∼11 Å, thereby minimizing any spurious interactions between neighboring slabs. The dimensions of the supercell were chosen to be consistent with the calculated conventional lattice parameter of 3.97 Å obtained using the GGA (experimental value 3.9236 Å[32]). This gave a supercell of dimensions 5.62 × 7.95 × 19.66 Å^3. Brillouin-zone integration was achieved by summation over a 4 × 3 × 1 Monkhorst−Pack mesh[33] of special **k** points. A Fermi-surface smearing of 0.2 eV was employed in the calculations, and the results were extrapolated to 0 K using the method of Gillan and de Vita.[34,35] Convergence with respect to **k**-point sampling, kinetic energy cutoff, and slab thickness was tested and found to be satisfactory. Increasing the **k**-point sampling mesh to 5 × 4 × 1 and the energy cutoff to 380 eV, for example, resulted in a difference of only 6 meV for the adsorption energy of CH on Pt{110}(1 × 2).

Adsorption was confined to one side of the slab for all calculations, with the adsorbate coverage corresponding to 0.25 ML in the initial state of the reaction (relative to the surface-layer Pt atom density on the unreconstructed surface). The dehydrogenation reactions were investigated using a constrained minimization technique in which the reaction coordinate was assumed to consist primarily of a C−H bond elongation. An initial approximation to the transition-state structure was obtained by appealing to analogous results for the Pt{111} system.[12−14] The structure was then refined by incrementally increasing or decreasing the active C−H bond length until the corresponding first-order saddle point was identified and the rms forces on the adsorbate and top three substrate layers fell below 0.04 eV/Å. Within the current methodology, the transition-state structure is identified as an energy maximum with respect to the C−H bond length of the dissociating bond and a minimum with respect to the remaining orthogonal adsorbate and substrate degrees of freedom and corresponds to a true first-order saddle point on the potential energy surface. The transition state was further verified by confirming that the relevant forces on the adsorbate changed sign on either side of the maximum. For all reactions, more than one transition-state structure was investigated to identify the lowest-energy structure for each reaction. We note that the constrained minimization approach has been successful in identifying reaction pathways and transition-state structures in a number of related systems.[8,12−14,16,17]

III. Methyl Dehydrogenation on Pt{110}(1 × 2)

A. CH_3 Dehydrogenation Reaction Pathway. The most stable site for the adsorption of CH_3 on Pt{110}(1 × 2) is the atop site situated on the ridge atoms of the missing-row reconstructed Pt{110}(1 × 2) surface.[28] The initial state for the dehydrogenation reaction was thus chosen to correspond to a methyl species adsorbed in this site (Figure 1a). Two pathways were considered in which the dissociating hydrogen atom was displaced either in the direction of the atop site on the adjacent ridge atom or in the direction of the atop site of a second-layer substrate atom on the {111} microfacet. The lowest-energy pathway identified is illustrated schematically in Figure 1, in which the "active" H atom is displaced in the direction of the neighboring ridge atop site. In this pathway and all subsequent pathways discussed in this paper, the initial and final states correspond to fully optimized structures (i.e., local minima on the potential energy surface) obtained by relaxing the constraint on the active C−H bond length.

In the low-energy pathway shown in Figure 1, the methyl moiety is initially located at the atop site (Figure 1a) and translates toward the bridge site as the C−H bond aligned along the close-packed row is stretched. As the methyl moiety migrates along the ridge, it passes through a local minimum (Figure 1b) that is raised in energy by 0.12 eV relative to the starting configuration (Figure 1a) and in which the CH_3 species is tilted toward the bridge site. The optimized adsorbate structure at this local minimum is characterized by a short (2.07 Å) and a long (2.36 Å) C−Pt bond with the active C−H bond stretched to 1.17 Å. In this geometry, the corresponding H−Pt distance to the neighboring ridge atom is reduced from 3.09 Å for CH_3 adsorbed in the atop site to 1.87 Å in the tilted configuration at the local minimum, which is suggestive of the formation of a stabilizing agostic interaction[36] between the methyl moiety and the surface. As the active C−H bond is stretched further, the transition state is accessed (Figure 1c), in which the C−H distance is elongated to 1.60 Å. At the end of the dissociation reaction, the nascent methylene remains in the bridge site, with the hydrogen adatom coadsorbed in the adjacent bridge site along the close-packed ridge (Figure 1d). Both species are thus chemisorbed in their respective lowest-energy adsorption sites in the final state,[28] for which a negligible interaction energy of 0.01 eV/(2 × 2) cell is obtained for the coadsorbed geometry,

TABLE 1: Selected Structural Parameters Characterizing the CH_3 Dehydrogenation Pathway Illustrated in Figure 1[a]

	d_{C-Pt_1}	d_{C-Pt_2}	$d_{\perp(C-surf)}$	d_{C-H}	d_{H-Pt_2}	α (deg)	β (deg)
(a)	2.05	3.55	2.05	1.09	3.09	17	32
(b)	2.07	2.36	1.73	1.17	1.87	4	63
(c)	2.04	2.11	1.54	1.60	1.61	3	82
(d)	2.04	2.04	1.50	2.86	1.76		90

[a] Pt_1 is the ridge atom to which methyl is adsorbed in the initial state, and Pt_2 is the neighboring ridge atom in the (2 × 2) unit cell. d_{C-H} and d_{H-Pt_2} refer to the dissociating hydrogen atom. α denotes the angle between the macroscopic surface plane and the C−H bond of the active hydrogen, and β denotes the angle between the macroscopic surface plane and the HCH plane of the inactive hydrogens. The transition state corresponds to (c). All distances are in angströms.

compared to the separate adsorption of CH_2 and H each at a local coverage of 0.25 ML.

Selected structural parameters characterizing the adsorbate geometry at each of the points illustrated in Figure 1 are summarized in Table 1. As the dissociation reaction proceeds, the C−Pt distance to the adjacent ridge atom (d_{C-Pt_2} in Table 1) is progressively shortened, and the HCH plane of the nondissociating hydrogen atoms moves into an orientation perpendicular to the macroscopic surface plane, as indicated by angle β in Table 1. At the transition state (Figure 1c), the CH_2 moiety is located close to the bridge site, with the remaining dissociating hydrogen atom close to an atop configuration. The active C−H bond is stretched to 1.60 Å and is aligned approximately parallel to the plane of the ridge, with a corresponding angle of 3° between the active C−H bond and the macroscopic surface plane. The transition-state geometry bears a strong structural resemblance to the methylene product state, which is further borne out by the electronic structure analysis discussed below.

The microscopic reaction pathway for methyl (de)hydrogenation on Pt{111} has recently been identified using periodic slab calculations within the framework of density functional theory.[12−14] A similar transition-state structure was reported in which the active C−H bond is stretched to 1.63 Å, with the heavier CH_2 fragment located close to a bridge site and the dissociating hydrogen located near the atop site. It is worth noting that in the transition states identified for methyl dehydrogenation on both Cu{111}[12] and Pd{100}[16] the dissociating hydrogen is located close to a bridge site and not an atop site. However, for atomic hydrogen adsorption on both of these surfaces, the atop site has been reported to be less stable by approximately 0.5 eV compared to the respective lowest-energy adsorption site.[12,16] In contrast, the potential energy surface determined for hydrogen adsorption is relatively flat both on Pt{111}[13] and in the region of the ridge sites on Pt{110}(1 × 2),[28] suggesting that the corrugation of the potential energy surface for hydrogen adsorption may influence the location of the dissociating hydrogen atom relative to the surface in the lowest-energy transition-state structure, as discussed previously.[13,15,16]

B. Reaction Energetics. The calculated activation energy for CH_3 dehydrogenation is 0.34 eV, which is significantly lower than the corresponding barrier of 0.83 eV determined for methyl dehydrogenation on Pt{111}.[12,13,14] The higher reactivity of the low-coordination ridge atoms on the reconstructed Pt{110}-(1 × 2) surface is thus borne out by the lower reaction barrier obtained for this surface. The increased reactivity of Pt{110}-(1 × 2) compared to that of Pt{111} for C−H bond activation has, for example, been noted in the context of alkane activation on both surfaces.[38]

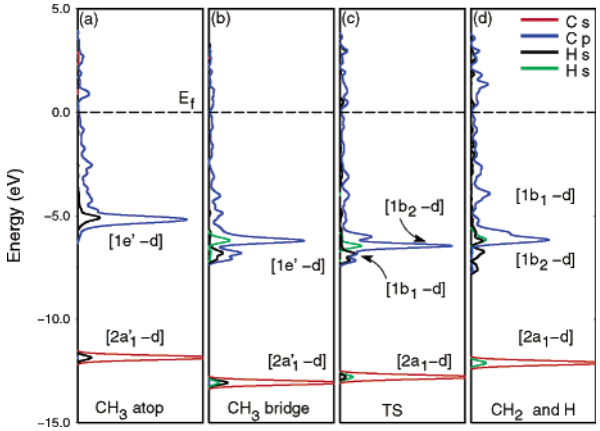

Figure 2. Projected density of states corresponding to the configurations shown in Figure 1 along the CH_3 dehydrogenation pathway. Projections onto the carbon 2s (red) and 2p (blue) states and the 1s states of the dissociating hydrogen (black) and the remaining equivalent hydrogen atoms (green) are shown for the (a) initial state, (b) local minimum near the bridge site, (c) transition state (TS), and (d) coadsorbed CH_2 and H. The curves have been referenced to the Fermi energy ($E_f = 0$).

The reaction enthalpy may be determined as the energy difference between the initial state and the final state with CH_2 and H coadsorbed in the same (2 × 2) surface unit cell, for which the corresponding enthalpy change is exothermic by 0.21 eV. Alternatively, the reaction enthalpy may be defined by

$$\Delta H = [E_{CH_2/Pt} + E_{H/Pt} - E_{Pt}] - E_{CH_3/Pt} \qquad (1)$$

where $E_{CH_2/Pt}$ and $E_{H/Pt}$ are the energies determined in separate calculations of CH_2 and H adsorbed in their respective lowest-energy adsorption sites on the Pt{110}(1 × 2) surface at a coverage of 0.25 ML; E_{Pt} is the energy of the relaxed clean surface, and $E_{CH_3/Pt}$ is the energy of the initial state with CH_3 adsorbed in the ridge atop site. The difference in enthalpy calculated using the two approaches is due to the interaction between the product moieties coadsorbed in the same (2 × 2) surface unit cell in the former case. For the CH_3 dehydrogenation pathway illustrated in Figure 1, the products are adsorbed in their respective lowest-energy sites[28] in the final state. The calculated interaction energy is negligible (0.01 eV) for this coadsorption geometry so that the reaction enthalpy is essentially the same within both definitions used above. It is worth noting that the corresponding enthalpy change calculated for this reaction on Pt{111}[13,14] is endothermic by 0.19 eV.

C. Bonding Analysis. The evolution of the electronic structure of the chemisorption system as the dehydrogenation reaction proceeds is embodied in the changes observed in the projected density of states (PDOS) shown in Figure 2 for different structural configurations along the reaction pathway. The electronic structure of CH_3 adsorbed in the atop site in the initial state (Figure 2a) has been discussed in detail in a separate publication.[28] In summary, the chemisorption of CH_3 to the surface is dominated by the interaction between the highest occupied molecular orbital (HOMO) of the CH_3 radical, the $1a_2''$ orbital, and the metal d states on the ridge atom of the atop site. The $2a_1'$ orbital and the degenerate pair of 1e′ valence orbitals of the methyl radical, which are lower in energy than the $1a_2''$ orbital, play a minor role in the net covalent bonding of the adsorbate to the surface.[28]

As the methyl moiety moves from the atop site into the local minimum near the bridge site, changes in the PDOS are evident, as shown in Figure 2b. Both the carbon s peak ~13 eV below

the Fermi energy (E_f) and the largest carbon p peak ~6 eV below E_f in Figure 2b have shifted down in energy by ~1 eV relative to their positions in Figure 2a. In addition, smaller peaks have separated out of the main carbon p peak and are shifted down to lower energies (~7 eV below E_f). The general downshift in energy of the peaks is indicative of a stabilization of the contributing adsorbate orbitals to the states within those peaks as the CH_3 moiety moves to the higher coordination site.

In the bridging geometry, the C−H bond aligned along the close-packed ridge is stretched to 1.17 Å. In this distorted adsorbate configuration, the $2a_1'$ methyl orbital, which interacts only weakly with the substrate in the initial state,[28] is more delocalized, suggesting that the kinetic energy of this state is lowered so that the corresponding peak is shifted down in energy relative to that shown in Figure 2a. Furthermore, the degeneracy of the two 1e′ methyl orbitals is broken in this site, and the 1e′ orbital aligned along the close-packed ridge interacts more strongly with the substrate orbitals than in the atop site. The smaller carbon p peaks in Figure 2b ~7 eV below the Fermi energy may be attributed to interactions of this type, as can be deduced from the additional contribution to the peak from the s orbital (black) of the dissociating hydrogen atom.

As the CH_3 moiety migrates toward the bridge site, the carbon atom moves closer to the surface by 0.32 Å (as indicated by the change in the vertical height of the carbon atom above the ridge plane, $d_{\perp(C-surf)}$ in Table 1), which allows for a more efficient overlap of the 1e′ orbitals with the substrate orbitals. However, the change in the adsorption site also alters the phase relationship between the adsorbate and substrate orbitals, and both effects determine the position of the corresponding 1e′-derived peaks in the PDOS. For the local minimum near the bridge site, the change in adsorption geometry appears to result in an increased stabilization of the bonding interaction for both 1e′ orbitals with the surface, but more so for the orbital aligned along the ridge.

The stabilization of the 1e′ orbital aligned along the Pt−Pt bond in methyl adsorbed in the bridge site on Pt{111} has been noted by Papoian et al.[39] in their detailed analysis of CH_3 adsorption on Pt{111}. It should be noted that the stabilization of some of the adsorbate orbitals does not imply that the system as a whole is lower in energy than for adsorption in the atop site. The additional contribution of the $1a_2''$ methyl orbital to the adsorbate system, which is the main contributor to the net covalent bonding of CH_3 to the surface,[28] and the effect of the adsorbate on the bonding interactions within the substrate will play a decisive role in determining the overall stability of the system.[39,40]

The PDOS of the transition-state geometry is shown in Figure 2c. The real-space distribution of individual quantum states localized on the heavier CH_2 fragment in the transition-state structure strongly resembles the states observed for methylene adsorbed in the ridge bridge site, as discussed previously[28] and summarized below (section 4.3). As the dehydrogenation reaction proceeds on the surface, the 1e′ orbital of the methyl species evolves into the $1b_1$ orbital of nascent methylene, which is stabilized by the surface. At the transition state, three-center bonds are formed that exhibit strong $1b_1$ orbital character, in which the electron density is distributed over the carbon, dissociating H, and ridge Pt atoms. The electron density distribution of such an eigenstate evaluated at $\bar{\Gamma}$ is shown in Figure 3a. This state contributes to the low-energy carbon p peak ~7 eV below E_f indicated in Figure 2c. Within the large carbon p peak (~6.5 eV below E_f), states of $1b_2$ character on the CH_2 fragment are evident, as shown in Figure 3b. States

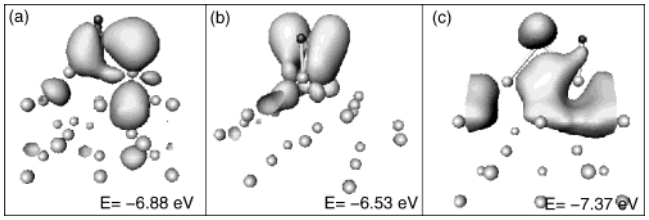

Figure 3. Isosurfaces of the electron density distribution of individual eigenstates evaluated at $\bar{\Gamma}$ for the transition state of the CH_3 dehydrogenation reaction. The isosurfaces correspond to an electron density of 6.8×10^{-3} electrons/Å^3. The angle of view in plots a and c is the same and is orientated in the [001] direction across the ridge, with the dissociating hydrogen atom positioned on the right of the image (small black sphere); plot b is viewed approximately down the close-packed ridge.

with strong $3a_1$ CH_2 orbital character are similarly found within this energy region, an example of which is shown in Figure 3c.

Throughout the dehydrogenation reaction, the valence orbitals of the distorted methyl moiety are able to interact with and be stabilized by the surface. In particular, the stabilization of both the reactant and product states on the surface results in an exothermic surface reaction (by 0.21 eV) compared to the corresponding gas-phase reaction that is calculated to be endothermic by 4.99 eV. The PDOS of the final state of the reaction with CH_2 and H coadsorbed in adjacent bridge sites is shown in Figure 2d. The projection onto the carbon states is qualitatively identical to that obtained for CH_2 adsorbed in the bridge site, as discussed previously[28] and summarized below (section 4.3). The bonding of the dissociated hydrogen atom to the surface in the adjacent bridge site is manifested in the projection onto the corresponding H s orbital in Figure 2d (black trace).

It is worth emphasising that the interaction of the organic fragment orbitals with the substrate orbitals results in the formation of both bonding and antibonding mixed states and that the net population of these states determines the net contribution of the fragment orbital to the adsorbate−substrate bond. The key molecular orbitals involved in the stabilization of the adsorbate on the surface are thus the frontier orbitals, which lie close in energy to the Fermi level and for which the antibonding combinations are predominantly pushed above the Fermi energy and depopulated, resulting in a net stabilizing contribution to the adsorbate−substrate bond.[41] The contribution of all populated states must be taken into account when assessing both the origin of the strength of the adsorbate bond to the surface and the stability of the system relative to other adsorption configurations.

IV. Methylene Dehydrogenation on Pt{110}(1 × 2)

A. CH_2 Dehydrogenation Reaction Pathway. The lowest-energy site for CH_2 adsorption on Pt{110}(1 × 2) is the bridge site on the ridge atoms of the missing-row reconstructed surface, with the HCH plane aligned in the [001] direction perpendicular to the close-packed rows.[28] For CH_2 adsorbed in this site in the initial state, two pathways were investigated in which the CH and H fragments were displaced either toward the same side or toward opposite sides of the close-packed ridge. The lower-energy pathway (by ~0.1 eV) is shown in Figure 4a−c (path I), in which the dissociation takes place over a second-layer substrate atom (Figure 4b) and the nascent CH and atomic H are adsorbed on the same side of the ridge in the final state (Figure 4c). In the transition-state geometry for this pathway (Figure 4b), the active C−H bond is stretched to 1.45 Å, and the corresponding H−Pt distance to the second-layer atom is

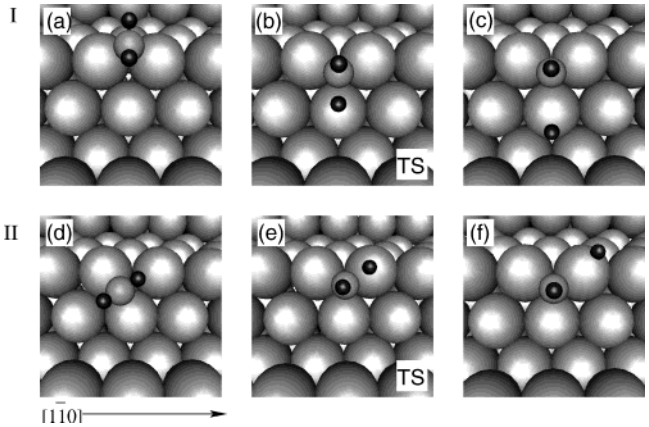

Figure 4. Methylene dehydrogenation reaction pathways on Pt{110}-(1 × 2) viewed in the direction normal to the {111} microfacet. (I) (a) Initial, (b) transition, and (c) final states of the higher-energy pathway; (II) (d) initial, (e) transition, and (f) final states of the lower-energy pathway. Color coding of atoms is as described in Figure 1.

TABLE 2: Selected Structural Parameters Characterizing the Two CH_2 Dehydrogenation Pathways Illustrated in Figure 4[a]

	d_{C-Pt_1}	d_{C-Pt_2}	d_{C-Pt_3}	$d_{\perp(C-surf)}$	d_{C-H}	d_{H-Pt_3}
(a)	2.02	2.02	3.31	1.45	1.09	3.32
(b)	2.00	2.00	2.15	1.20	1.45	1.65
(c)	1.99	1.99	2.03	1.12	2.67	1.60
(d)	2.05	2.05	2.94	1.54	1.09	2.71
(e)	2.00	2.03	2.10	1.20	1.45	1.64
(f)	1.99	2.01	2.01	1.16	2.89	1.58

[a] (a−c): Dehydrogenation over the second-layer atom on the {111} microfacet (path I); (d−f) dehydrogenation over the ridge atom of the 3-fold site (path II). Pt_3 is the atom over which hydrogen dissociates in each reaction, and Pt_1 and Pt_2 label the remaining atoms of the 3-fold site. $d_{\perp(C-surf)}$ is the perpendicular height of the carbon atom above the local surface plane; d_{C-H} and d_{H-Pt_3} refer to the active H. All distances are in angströms.

1.65 Å. The dissociating hydrogen is thus close to an atop configuration. At the end of the reaction, the nascent methylidyne moiety is adsorbed in the fcc 3-fold site with the C−H axis aligned perpendicular to the {111} microfacet (to within less than 1°). The dissociated hydrogen atom is located close to the atop site at a H−Pt distance of 1.60 Å and at an angle of 38° to the microscopic surface normal. Selected structural parameters characterizing this reaction pathway are summarised in Table 2, (a)−(c).

It is reasonable to expect that an analogous structure to that depicted in Figure 4b, corresponding to dissociation over a ridge Pt atom rather than a second-layer atom, may lead to a lower-energy pathway. Indeed, the investigation of such an alternative geometry resulted in the identification of the transition-state structure depicted in Figure 4e, in which the energy is lowered by 0.21 eV relative to that of the former structure illustrated in Figure 4b. In this transition-state structure, the active C−H bond is similarly stretched to 1.45 Å, with a corresponding H−Pt distance of 1.64 Å. Incremental contraction of the active C−H bond until the initial state is reached reveals that such a transition structure is accessed from a neighboring local minimum in which the CH_2 species is chemisorbed in the higher-energy bridge site (by 0.42 eV[28]) on the {111} facet and not from the ridge bridge site. The corresponding dehydrogenation pathway, including the final state, is shown in Figure 4d−f (path II), and selected structural parameters characterizing this alternative pathway are summarized in Table 2.

When considering the fate of CH_2 adsorbed in the ridge bridge site, it is useful to take into account the competing process of diffusion into an adjacent bridge site on the {111} facet, from which dissociation can take place via the lower-energy transition structure. The calculation of the corresponding diffusion pathway indicates that the energy barrier for diffusion into the neighboring facet bridge site is ∼0.1 eV lower than for direct dissociation via the higher-energy transition state (Figure 4b). It is therefore energetically preferable for CH_2 dehydrogenation to take place via diffusion into the facet bridge site with subsequent dissociation from this site, as illustrated in path II (Figure 4). Indeed, the lower-energy transition structure may even be directly accessible from the ridge bridge site with no additional energy cost, although we are unable to present direct evidence in support of this within the current methodology.

B. Reaction Energetics. For path I, the calculated activation energy is 0.77 eV relative to CH_2 adsorbed in the ridge bridge site in the initial state, and the enthalpy change is endothermic by 0.32 eV for CH and H coadsorbed in the (2 × 2) surface unit cell in the final state. With subsequent diffusion of atomic hydrogen into the lowest-energy adsorption site in islands with a local coverage of 0.25 ML, the overall enthalpy change for this reaction is exothermic by 0.16 eV. However, if the lower-energy transition state (Figure 4e) is directly accessible from the lowest-energy ridge bridge site (Figure 4a) with no additional barrier, then the activation energy for dehydrogenation is reduced to 0.56 eV. It is worth noting that for CH_2 adsorbed in the facet bridge site (Figure 4d), which is 0.47 eV less stable than the ridge bridge site, the barrier to dissociation is only 0.09 eV.

Watson et al.[1,7] performed a kinetic analysis of the results of hydrogen−deuterium exchange experiments for methylidyne adsorbed on Pt{110}(1 × 2), from which an activation barrier of 70 kJ mol^{-1} was estimated for the surface $CH_a + D_a \rightleftharpoons CHD_a^{\ddagger} \rightleftharpoons CD_a + H_a$ exchange reaction. This result may be compared with the present calculated activation energy for the reverse association reaction in which CH is rehydrogenated to chemisorbed CH_2 (neglecting zero-point vibrational energy corrections). For the association reaction, the lower-energy transition-state geometry (Figure 4e) is directly accessible, and the corresponding calculated activation energy is 0.16 + 0.56 = 0.72 eV (69 kJ mol^{-1}). The calculated activation energy is thus in remarkably good agreement with the experimentally estimated value.

Interestingly, the calculated barrier of 0.14 eV obtained for CH_2 dehydrogenation on Pt{111}[13,14] is considerably lower than that found on the Pt{110}(1 × 2) surface in the present work, despite the fact that the transition-state geometry is very similar on both surfaces. The calculated chemisorption energy for CH_2 adsorbed in the bridge site on Pt{111} is, however, 4.06 eV, which is 0.55 eV lower than for CH_2 adsorption in the ridge bridge site on Pt{110}(1 × 2).[28] The higher dehydrogenation barrier on Pt{110}(1 × 2) relative to that on Pt{111} is thus due in part to the increased stabilization experienced by CH_2 adsorbed on the ridge site on Pt{110}(1 × 2). Indeed if the dehydrogenation pathway is confined to the microfacet (path II in Figure 4), then the corresponding energy barrier of 0.09 eV is similar to that calculated for Pt{111}.

C. Bonding Analysis. The bonding of CH_2 to the Pt{110}(1 × 2) surface has been analyzed in detail previously[28] for the case of CH_2 adsorbed in the ridge bridge site with carbon in a tetrahedral environment. The projected density of states (PDOS) for this adsorption configuration is shown in Figure 5a. For CH_2 adsorbed in the bridge site on the {111} microfacet, an

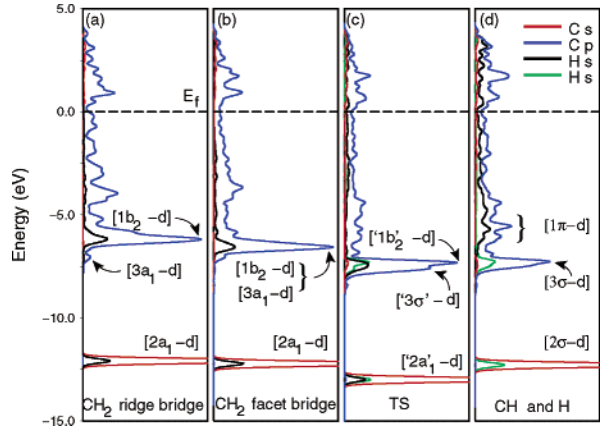

Figure 5. Projected density of states for configurations along the CH_2 dehydrogenation pathway. Projections onto the carbon 2s (red) and 2p (blue) states and the 1s orbitals of the dissociating (black) and inactive (green) hydrogen atoms are shown for CH_2 adsorbed in the (a) ridge bridge site, (b) microfacet bridge site, (c) low-energy transition state (TS), and (d) final state with CH in the 3-fold site and hydrogen near the ridge atop site. The curves have been referenced to the Fermi energy ($E_f = 0$).

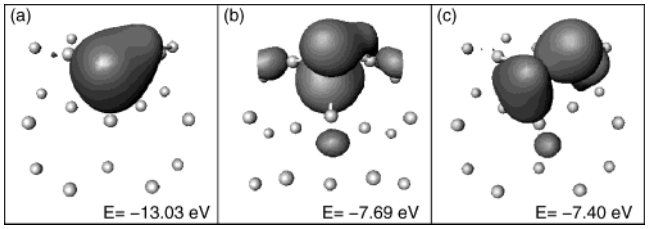

Figure 6. Isosurfaces of the electron density distribution of individual eigenstates evaluated at $\bar{\Gamma}$ for the low-energy transition state of the CH_2 dehydrogenation reaction. The isosurfaces correspond to an electron density of 1.1×10^{-2} electrons/Å^3. The adsorbate is viewed in the same orientation as in Figure 4e.

analogous interpretation of the projection of the total density of states onto the valence atomic orbitals of the adsorbate is applicable (Figure 5b). The PDOS in Figure 5b is characterized by a low-energy peak (∼12.3 eV below E_f) that contains states of $2a_1$ character predominantly localized on the adsorbate and a large carbon p peak (∼6.6 eV below E_f) containing states derived from both the $3a_1$ and $1b_2$ molecular orbitals of the CH_2 radical. Further interactions due to the $1b_1$ orbital of the CH_2 radical are distributed throughout the energy interval from −5 eV up to the Fermi level, with unoccupied antibonding states derived from the $1b_1$ and $3a_1$ orbitals occurring above E_f.

To illustrate what happens during the CH_2 dehydrogenation reaction, we focus our attention on path II (Figure 4), accessed through the C−H stretch. The evolution of the electronic structure of the chemisorption system along the methylene dehydrogenation reaction pathway is embodied in the PDOS in Figure 5b−d for the reaction on the microfacet (path II in Figure 4d−f). At the transition state, the $2a_1$ peak is shifted down in energy by ∼0.8 eV presumably because of the delocalization of this state over the distorted CH_2 moiety, leading to a decrease in kinetic energy. The real-space distribution of the $2a_1$-derived state evaluated at $\bar{\Gamma}$ is shown in Figure 6a.

During the dehydrogenation reaction, the orbitals of the CH_2 moiety rehybridize, thereby giving rise to the molecular orbitals of the reaction products, CH and H, which mix with the metal states. The orbital features of the product state are already apparent in the transition-state geometry, with states with the 3σ orbital character of the CH product occurring at low energies (∼7.7 eV below E_f), as shown in Figure 6b. In addition, the

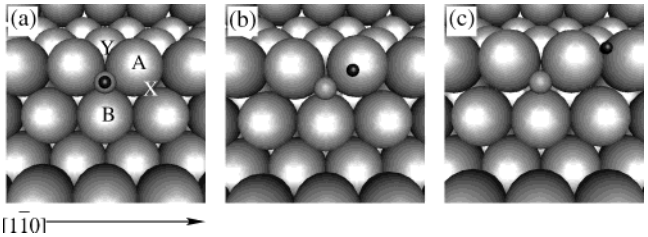

Figure 7. Methylidyne dehydrogenation reaction pathway on Pt{110}-(1 × 2) viewed in the direction normal to the {111} microfacet. (a) Initial state, (b) transition state, and (c) final state with coadsorbed carbon (small gray sphere) and H (black sphere).

orbital character of the parent moiety is still evident in the transition-state geometry, as indicated by the strong $1b_2$ orbital character of the state shown in Figure 6c, which contributes to the main carbon p peak in Figure 5c ∼7.4 eV below E_f. The dominant low-energy carbon p peak in Figure 5c (∼7.5 eV below E_f) is shifted down in energy relative to the corresponding peak ∼6.6 eV below E_f for the initial-state geometry (Figure 5b). The rehybridization of the adsorbate orbitals, in combination with a change in adsorption site and a reduction of the vertical height of the distorted CH_2 species above the macroscopic surface plane (Table 2), determines the extent of the interaction of the rehybridized adsorbate orbitals with the substrate states and the corresponding energy of the resulting mixed states. Of particular significance is the fact that the quantum states derived from the adsorbate orbitals are stabilized through interaction with the substrate states throughout the reaction so that the maximum increase in energy along the reaction pathway, as represented by the activation energy, is significantly reduced compared to the significant increase in energy for the analogous gas-phase dissociation reaction.

The dissociation of CH_2 to CH and H in the gas phase is endothermic by 4.39 eV[32] (calculated endothermicity 4.89 eV). For the surface reaction, the endothermicity is significantly reduced by the stabilization of both the reactant and the product moieties on the surface as a result of mixing between the adsorbate orbitals and the substrate states in each case. For the surface reaction, the $1b_2$ and $3a_1$ orbitals of CH_2 are transformed into one of the 1π orbitals and the 3σ orbital of methylidyne and the 1s orbital of H in the final state. The transformation of the CH_2 $1b_2$ orbital into a CH 1π state is accompanied by an enhanced contribution of this orbital to the adsorbate−substrate bond. As a result, the surface alkylidene bond characteristic of chemisorbed CH_2 is transformed into an alkylidyne bond for adsorbed CH in the final state.

V. Methylidyne Dehydrogenation on Pt{110}(1 × 2)

A. CH Dehydrogenation Reaction Pathway. Methylidyne dissociation to chemisorbed carbon and hydrogen was investigated for CH adsorbed in the lowest-energy adsorption site, the fcc 3-fold site on the {111} microfacet,[28] in the initial state. Dehydrogenation pathways were investigated in which the dissociating hydrogen atom was displaced in the direction of either of the two inequivalent Pt atoms of the 3-fold site (A and B in Figure 7a) or in the direction of the next-nearest-neighbor bridge site on the {111} microfacet (X in Figure 7a) and the nearest bridge site on the close-packed ridge (Y in Figure 7a).

The lowest-energy dehydrogenation pathway identified is illustrated schematically in Figure 7, in which the initial, transition, and final-state geometries are shown. In this pathway, methylidyne is initially located in the fcc 3-fold site on the {111}

TABLE 3: Selected Structural Parameters Characterizing the CH Dehydrogenation Pathway Illustrated in Figure 7 for the Initial State (a), Transition State (b), and Final State (c) of the Reaction[a]

	d_{C-Pt_1}	d_{C-Pt_2}	d_{C-Pt_3}	$d_{\perp(C-surf)}$	d_{C-H}	d_{H-Pt_1}
(a)	2.00	2.00	2.00	1.16	1.09	2.78
(b)	1.97	1.92	1.91	0.87	1.57	1.65
(c)	1.92	1.90	1.91	0.80	3.19	1.78

[a] Pt atoms of the 3-fold site are numbered clockwise from the ridge atom over which the hydrogen atom dissociates. $d_{\perp(C-surf)}$ is the perpendicular height of the carbon adatom above the plane of the substrate atoms of the 3-fold site. All distances are in angströms.

microfacet, with the C−H axis aligned approximately perpendicular to the microscopic surface plane (Figure 7a). The dissociating hydrogen atom is displaced toward one of the ridge atoms of the 3-fold site in the transition state, and the carbon atom remains in the hollow site (Figure 7b). In the final state, the hydrogen atom is located in the adjacent ridge bridge site with the carbon atom coadsorbed in the fcc 3-fold hollow site (Figure 7c). The interaction energy for this coadsorption configuration is repulsive by 0.05 eV, relative to the separate adsorption of atomic C and H in the same sites at a local coverage of 0.25 ML. It should be noted that in the final state the carbon adatom is not located in its lowest-energy site on the Pt{110}(1 × 2) surface, which is the pseudosubsurface 4-fold site located below the long-bridge site in the trough.[28] The carbon adatom may thus be expected to diffuse into the lower-energy site after the dissociation reaction is complete.

Selected structural parameters characterizing the dehydrogenation pathway are summarized in Table 3. As the dissociation reaction proceeds, the C−Pt bond distance is reduced from 2.00 Å, characteristic of CH adsorbed in the 3-fold site in the initial state, to ∼1.91 Å for chemisorbed carbon in the final state. More significant is the change in the vertical height of the carbon adatom above the microscopic plane of the {111} microfacet. As the dissociation reaction proceeds, the carbon atom sinks toward the microscopic surface plane until at the transition state the adatom is located 0.29 Å closer to the hollow site than in the initial state. In response, the three substrate atoms of the hollow site move apart to accommodate the carbon atom. In the transition state, the carbon atom is in a geometry that more closely approximates the final state than the initial state. Only the C−Pt bond that is shared with the dissociating hydrogen atom is significantly distorted to 1.97 Å compared to the final-state bond distance of 1.92 Å, which is characteristic of bond competition between the carbon and hydrogen atoms interacting with the same substrate atom. The transition-state C−H bond distance is 1.57 Å, with a corresponding H−Pt distance of 1.65 Å.

It is worth noting that the structurally similar transition state corresponding to dehydrogenation over the second-layer Pt atom of the 3-fold site results in a pathway that is 0.11 eV higher in energy than the lowest-energy pathway identified. In the corresponding transition state, the C−H bond is stretched to 1.60 Å with a corresponding H−Pt distance of 1.63 Å, and the C−Pt distance to the shared Pt atom is similarly elongated compared to the remaining C−Pt bonds of the 3-fold site.

The lowest-energy transition state reported for the reverse process of carbon hydrogenation on Pt{111}[13,14] is structurally equivalent to the transition state identified in the present study for CH dehydrogenation on Pt{110}(1 × 2). Similar transition-state geometries in which the hydrogen atom is located close to a top site and the carbon adatom is located in a 3-fold site have been reported for carbon hydrogenation on Ni{111},[8] Pd{111},[17] Rh{111},[17] and Ru{0001}.[17] However, for the corresponding reactions on Cu{111}[13,15] and Pd{001},[16] the hydrogen atom was reported to be located close to a bridge site, as similarly noted in section 3.1 for the case of methyl dehydrogenation on these surfaces.

B. Reaction Energetics. The calculated activation energy for CH dehydrogenation is 1.20 eV (116 kJ mol^{-1}). Watson[1] determined an activation barrier of 1.25 eV (121 ± 3 kJ mol^{-1}) for methylidyne dehydrogenation on Pt{110}(1 × 2) using temperature-programmed reaction spectroscopy. The calculated activation energy for the surface dissociation reaction is thus in excellent agreement with the experimentally determined value. Zhang and Hu[16] recently reported a variation of as much as 0.2 eV between the reaction barriers calculated with the PW91[30] and the revised Perdew−Burke−Ernzerhof (RPBE) exchange-correlation energy functionals[42] for CH_x ($x = 1-4$) dehydrogenation on Pd{001}. With this in mind, the calculated and experimentally determined activation energies for CH dissociation on Pt{110}(1 × 2) are in agreement to within the intrinsic uncertainty of both approaches used.

The calculated enthalpy change for the dissociation reaction, evaluated as the energy difference between the initial and final states with carbon and hydrogen coadsorbed in the (2 × 2) surface unit cell in the latter case, is endothermic by 0.53 eV. The coadsorption configuration of the final state (Figure 7c) is characterized by a repulsive interaction energy of 0.05 eV so that the endothermicity of the reaction is reduced to 0.48 eV for separate adsorption in the same sites for each product at a local coverage of 0.25 ML. Considering carbon diffusion into the lowest-energy 4-fold site in the trough, the calculated endothermicity is further reduced to 0.38 eV if atomic hydrogen remains adsorbed on the surface.

The calculated activation energy of 1.53 eV for CH dissociation on Pt{111}[13,14] is considerably higher than that determined in the present study on Pt{110}(1 × 2). The endothermicity of the reaction is also found to be greater on Pt{111}, with a calculated value of 0.75 eV being obtained for the surface dissociation reaction.[13,14] The increased reactivity of Pt{110}-(1 × 2) relative to Pt{111} for C−H bond activation is thus further extended to the methylidyne dehydrogenation reaction.

C. Bonding Analysis. In the gas phase, the dissociation of CH into atomic carbon and atomic hydrogen is an endothermic process by 3.51 eV[32] (calculated endothermicity 3.70 eV) in which both the 2σ and 3σ bonding molecular orbitals of the CH radical are transformed into the higher-energy atomic orbitals of the products. For the chemisorption system, however, the interaction of the adsorbate orbitals with the Pt substrate states results in a reduction in the overall endothermicity of the dehydrogenation reaction to 0.53 eV for the coadsorbed final state, as discussed above. This overall lowering of the energy change may be rationalized by appealing to the detailed electronic structure of the chemisorbed system at key points in the dehydrogenation reaction.

For the chemisorbed system, the projections of the total density of states onto the carbon 2s and 2p orbitals and the 1s orbital of the hydrogen atom are shown in Figure 8 for the initial, transition, and final states of the methylidyne dehydrogenation reaction. The electronic structure of CH adsorbed in the fcc 3-fold hollow site in the initial state (Figure 8a) has been discussed in detail previously.[28] To summarize, on adsorption of the organic fragment on the surface, the 3σ orbital of the CH fragment is significantly stabilized and lowered in energy. In contrast, the 2σ orbital is largely unaffected by the surface, experiencing only a weak net covalent interaction with the

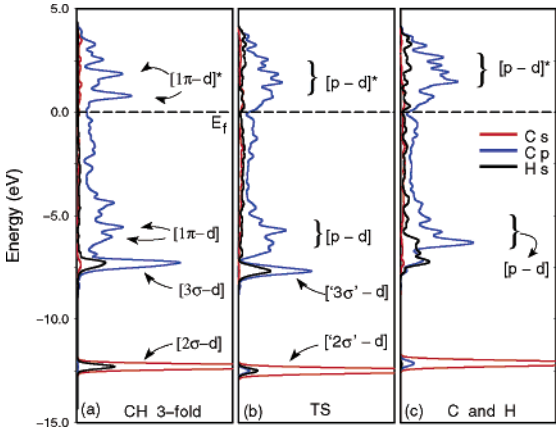

Figure 8. Projected density of states for each of the configurations shown in Figure 7 along the CH dehydrogenation pathway. Projections onto the carbon 2s (red) and 2p (blue) states and the 1s orbital of hydrogen (black) are shown for the (a) initial state, (b) transition state (TS), and (c) final state with coadsorbed carbon and hydrogen. The curves have been referenced to the Fermi energy ($E_f = 0$).

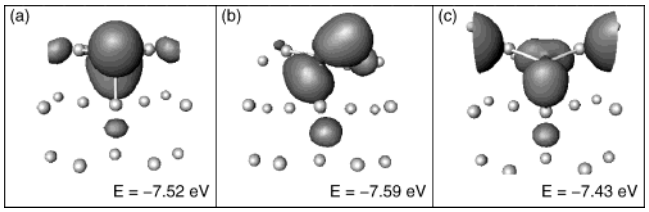

Figure 9. Isosurfaces of the electron density for eigenstates evaluated at $\bar{\Gamma}$ for the (a) initial-state, (b) transition-state, and (c) final-state geometries. The isosurfaces correspond to an electron density of 1.7 × 10^{-2} electrons/Å^3 and are viewed in the direction normal to the {111} microfacet in the same orientation as in Figure 7.

substrate orbitals of the 3-fold site. The dominant contribution to the formation of the covalent adsorbate−substrate bond originates from the degenerate 1π orbitals of the organic fragment mixing with the substrate states.

In the transition-state geometry, the projected density of states (PDOS) retains the qualitative features of the corresponding projection for the initial state. The [2σ-d] peak in Figure 8a is shifted slightly down in energy to ∼12.5 eV below E_f in the transition-state geometry (Figure 8b). Visualization of the real-space distribution of the quantum states within this peak suggests that these states retain much of the 2σ orbital character of the organic fragment, although rehybridization is apparent as indicated by the appearance of a nonnegligible projection onto the carbon p states for this peak in Figure 8b. The large carbon p peak ∼7.6 eV below E_f may similarly be associated with the [3σ-d] peak in the PDOS of methylidyne chemisorbed in the initial state. A representative state from within this peak evaluated at $\bar{\Gamma}$ is shown in Figure 9b (viewed with the same orientation as in Figure 7b), in which the electron density is predominantly localized on the distorted CH fragment and the presence of a three-center bond between the carbon, hydrogen, and one of the ridge Pt atoms is evident. In the gas phase, the 2σ and 3σ orbitals of methylidyne are raised in energy as the radical is distorted into the transition-state structure. On the surface, however, rehybridization of the orbitals within the fragment and mixing of the fragment orbitals with those of the substrate enable these states to remain low in energy, thereby contributing to the lowering of the overall energy barrier to dissociation relative to that of the gas-phase reaction. The evolution of a [3σ-d] state during the surface reaction is demonstrated in Figure 9.

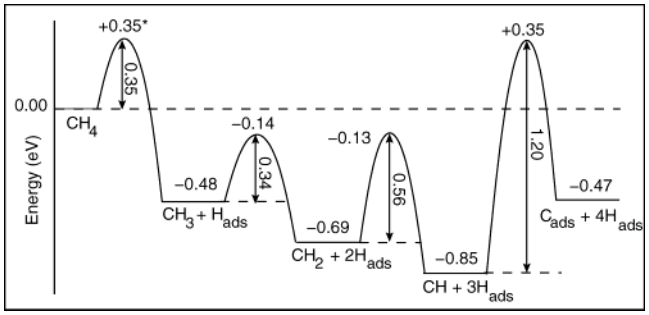

Figure 10. Reaction-energy profile for the transformation of CH_4 to carbon and hydrogen chemisorbed on the Pt{110}(1 × 2) surface. All energies are referenced to methane in the gas phase and the clean Pt{110}(1 × 2) surface. The activation barrier for CH_4 dissociative adsorption to chemisorbed CH_3 and H_{ads} (*) has been calculated in a separate study[43] and is included here for completeness.

In addition to the orbital interactions described above, the remaining p orbitals of the carbon atom contribute to the stabilization of the adsorbate on the surface. Bonding interactions between the carbon p orbitals and the substrate valence d orbitals are found within the energy interval of ∼7.2 to ∼4.3 eV below E_f for each of the projections in Figure 8. Corresponding antibonding interactions are dispersed throughout the energy interval above the Fermi energy. These interactions are particularly relevant to the bonding of the carbon adatom to the surface in the final state.

VI. Discussion

The reaction profile for CH_3 decomposition to atomic carbon on Pt{110}(1 × 2) is summarized in Figure 10. The first step in the dissociative adsorption of CH_4 on Pt{110}(1 × 2) to yield chemisorbed methyl (CH_3) is the subject of a separate theoretical study[43] in which the lowest-energy transition state for CH_4 dehydrogenation has been located using constrained minimization, by analogy to the determination of the dehydrogenation reaction pathways presented in the current work. The reported activation barrier for this dehydrogenation reaction is 0.35 eV[43] and corresponds to dissociation over the close-packed Pt ridge, resulting in CH_3 chemisorbed in the ridge atop site in the product state. This initial activated dissociation step has been included in Figure 10 for completeness.

In the reaction-energy profile shown in Figure 10, all energies are referenced to isolated gas-phase methane and the clean, relaxed Pt{110}(1 × 2) surface. For each of the stable dissociation intermediates, the energy corresponds to adsorption in the most stable site, and hydrogen coadsorption on the surface is assumed, as calculated in a separate unit cell with a local adatom coverage of 0.25 ML. For CH_2 dehydrogenation, the reaction barrier corresponds to dehydrogenation via the lowest-energy transition-state structure identified on the surface and neglects the possibility of additional energy barriers incurred for dissociation from the ridge bridge site, as discussed in section 4.1.

It is of interest to relate the energy profile in Figure 10 to the results of previous molecular beam experiments for this system.[1,3−7] The primary experimental observation of relevance is the identification of methylidyne as the stable surface dissociation intermediate in the surface-temperature range of 300−450 K, with the decomposition of CH to carbon and gaseous H_2 being observed above 470 K. It is important to note that in the molecular beam experiments the dissociation intermediates are identified indirectly by observing the product hydrogen gas desorbing from the surface, so that information

about the surface products of methane dissociation adsorption is necessarily restricted to temperatures above the hydrogen desorption temperature (i.e., restricted to surface temperatures for which the rate of recombinant desorption of hydrogen is rapid on the time scale of the experiment). No direct information is therefore obtained about the identity and relative concentration of the dissociation intermediates on the surface at temperatures below the hydrogen desorption temperature. Such information would in principle be accessible experimentally using surface spectroscopic techniques. It should also be noted that in the molecular beam experiments the desorbing H_2 gas is pumped away so that the surface dehydrogenation reactions may in theory be driven to completion. In the closed system at equilibrium, the Boltzmann distribution of the products is based on the free energies. This equilbrium distribution of the products will be perturbed by the entropy contribution of the gas-phase hydrogen once the temperature is raised above the hydrogen desorption temperature. Under the experimental conditions in which the hydrogen gas is pumped away from the chamber, however, equilibrium is reached only once the hydrogen gas has been completely removed, that is, when the surface decomposition reactions have been driven to completion and only adsorbed carbon remains on the surface. At temperatures both above and below the hydrogen desorption temperature, the rate of approach to equilibrium is governed by a combination of the rate of the final reaction step, in which CH is dehydrogenated to chemisorbed carbon and hydrogen adatoms, and the rate of recombinative hydrogen desorption from the surface.

In terms of the calculated relative stability of CH_x ($x = 0-3$) intermediates adsorbed on the surface in their respective lowest-energy sites, chemisorbed CH is found to be the most stable methane dissociation intermediate on this surface (Figure 10). The (indirect) observation of chemisorbed CH in the molecular beam experiments, however, is governed by the kinetics of both the surface CH_x decomposition reactions and the subsequent recombinant desorption of hydrogen from the surface. We note that the reaction-energy profile in Figure 10 is entirely consistent with the results obtained from previous molecular beam experiments. For CH dehydrogenation, the calculated activation energy of 1.20 eV (116 kJ mol^{-1}) is in excellent agreement with the experimentally determined value of 1.25 eV (121 ± 3 kJ mol^{-1}) and is consistent with the experimental observation of a high-temperature ($T \approx 470$ K) reaction-limited hydrogen desorption peak using temperature-programmed reaction spectroscopy.[1,6] At lower temperatures ($T \approx 310$ K), a single desorption-limited hydrogen peak is observed experimentally,[1,6] corresponding to the desorption of hydrogen produced from the dissociative adsorption of CH_4 and the subsequent surface dehydrogenation of CH_3 and CH_2 to methylidyne.

It is worth noting, however, that in an experimental investigation of the chemisorption of hydrogen on Pt{110}(1×2) using thermal desorption mass spectrometry[44] the activation energy for hydrogen desorption was reported to be strongly dependent on coverage and was found to vary from 1.15 eV (111 kJ mol^{-1}) to 0.56 eV (54 kJ mol^{-1}). For CH_2 dehydrogenation, the calculated activation energy is 0.56 eV (54 kJ mol^{-1}) for the low-energy pathway relative to that for CH_2 in the ridge bridge site. Thus, the activation energy calculated for CH_2 decomposition is comparable to the low-energy range of the activation energy for the hydrogen recombinant desorption reaction determined by Engstrom et al.[44] It should be noted that the kinetics of hydrogen desorption may further be influenced by the presence of CH_x intermediates coadsorbed on the surface. Nevertheless, the DFT results suggest that the experimentally observed single desorption peak at ~310 K is likely to be a convolution of both the (hydrogen) desorption-limited and (CH_2 dehydrogenation) reaction-limited peaks.

Of further interest is the experimental observation that chemisorbed CH can be deuterated to produce gas-phase CHD_3 and CD_4, whereas the deuteration of surface carbon is not observed experimentally.[1,7] Considering the reaction-energy profile in Figure 10, the calculated energy barrier for the surface hydrogenation of chemisorbed methylidyne to CH_2 is 0.72 eV (section 4.2), which is in good agreement with the experimentally estimated barrier.[1,7] Similarly, the activation barrier for the hydrogenation of carbon chemisorbed in the 3-fold site on the {111} microfacet on the Pt{110}(1×2) surface is 0.72 eV, as obtained by considering the reverse of the methylidyne dehydrogenation reaction discussed in section 5.2. Thus, if it is possible to rehydrogenate adsorbed methylidyne under the experimental conditions used in the molecular beam experiments[1,7] (high-flux deuterium beam at 370 K), then rehydrogenation of carbon chemisorbed in the 3-fold site should also be possible in principle.

However, the lowest-energy site for atomic carbon adsorption on the Pt{110}(1×2) surface is the pseudosubsurface 4-fold site in the trough,[28] and the fcc 3-fold site is calculated to be only 0.11 eV higher in energy.[28] Because there are twice as many fcc 3-fold sites on the surface as trough sites, the thermal population of the fcc 3-fold sites, in which carbon is reactive to rehydrogenation, may be expected to be appreciable in the upper limit of the temperature range of 250−700 K investigated experimentally. (Approximately 20% of the carbon adatoms may be expected to occupy the fcc site under equilibrium conditions at 650 K.) However, at high temperatures well above the hydrogen desorption temperature, the steady-state coverage of atomic hydrogen on the surface is presumably insufficient for the rehydrogenation of carbon to be observed experimentally. Conversely, at lower surface temperatures, the thermal population of the fcc 3-fold site is reduced so that the rehydrogenation of carbon in the 3-fold site is not observed over the entire temperature range examined experimentally. This interpretation of the experimental results does, however, rest upon the assumption that carbon adsorbed in the lowest-energy trough site is inactive to hydrogenation at these surface temperatures. It should also be noted that carbon is observed to lift the (1×2) reconstruction partially with increasing coverage[1,3] and that the additional possible formation of inert species (such as graphitic carbon) during the preparation of the carbon overlayer, which necessarily involves heating the surface to temperatures above 500 K, cannot be directly excluded.

VII. Conclusions

Density functional theory calculations have been used to determine the reaction pathways for CH_x ($x = 1-3$) dehydrogenation on the Pt{110}(1×2) surface. For each reaction, the dissociating hydrogen atom is located close to an atop site in the lowest-energy transition-state structure identified, with an energetic preference being observed for dissociation over a ridge Pt atom in each case. The calculated activation energy for CH_3 dehydrogenation is 0.34 eV, whereas for CH_2 dehydrogenation, the lowest-energy transition state identified is 0.56 eV higher in energy than CH_2 adsorbed in the most stable bridge site on the close-packed ridge. For CH dehydrogenation, the calculated activation barrier of 1.20 eV (116 kJ mol^{-1}) is in excellent agreement with the experimentally determined barrier of 1.25 eV (121 ± 3 kJ mol^{-1}). Similarly, for the reverse CH hydrogenation reaction, the calculated lowest-energy barrier of

0.72 eV is in good agreement with the corresponding experimentally estimated barrier.[1,7] The reaction-energy profile obtained for the conversion of chemisorbed CH_3 to CH and ultimately carbon on Pt{110}(1 × 2) is entirely consistent with the results of previous molecular beam experiments for this system.

Acknowledgment. We acknowledge financial support for this work from the EPSRC (U.K.) in the form of funds for workstations. M.A.P. thanks the Oppenheimer Trust for a research studentship and both the Cambridge Commonwealth Trust and the ORS Awards Scheme for financial assistance. S.J.J. thanks the Royal Society for a University Research Fellowship.

References and Notes

(1) Watson, D. T. P. Ph.D. Thesis, University of Cambridge, Cambridge, U.K., 2001.
(2) Walker, A. V.; King, D. A. *J. Phys. Chem. B* **2000**, *104*, 6462.
(3) Watson, D. T. P.; van Dijk, J.; Harris, J. J. W.; King, D. A. *Surf. Sci.* **2002**, *506*, 243.
(4) Walker, A. V.; King, D. A. *Phys. Rev. Lett.* **1999**, *82*, 5156.
(5) Walker, A. V.; King, D. A. *J. Chem. Phys.* **2000**, *112*, 4739.
(6) Watson, D. T. P.; Titmuss, S.; King, D. A. *Surf. Sci.* **2002**, *505*, 49.
(7) Watson, D. T. P.; Ge, Q.; King, D. A. *J. Chem. Phys.* **2001**, *115*, 11306.
(8) Watwe, R. M.; Bengaard, H. S.; Rostrup-Nielsen, J. R.; Dumesic, J. A.; Nørskov, J. K. *J. Catal.* **2000**, *189*, 16.
(9) Michaelides, A.; Hu, P. *J. Chem. Phys.* **2000**, *112*, 8120.
(10) Ciobîcă, I. M.; Frechard, F.; van Santen, R. A.; Kleyn, A. W.; Hafner, J. *J. Phys. Chem. B* **2000** *104*, 3364.
(11) Ciobîcă, I. M.; van Santen, R. A. *J. Phys. Chem. B* **2002**, *106*, 6200.
(12) Michaelides, A.; Hu, P. *J. Chem. Phys.* **2001**, *114*, 2523.
(13) Michaelides, A.; Hu, P. In *Theoretical Aspects of Heteogeneous Catalysis*; Nascimento, M. A. C., Ed.; Kluwer Academic Publishers: Dordrecht, The Netherlands, 2001.
(14) Michaelides, A.; Hu, P. *J. Am. Chem. Soc.* **2000**, *122*, 9866.
(15) Michaelides, A.; Hu, P. *J. Chem. Phys.* **2001**, *114*, 5792.
(16) Zhang, C. J.; Hu, P. *J. Chem. Phys.* **2002**, *116*, 322.
(17) Liu, Z.-P.; Hu, P. *J. Chem. Phys.* **2001**, *115*, 4977.
(18) Liu, Z.-P.; Hu, P. *J. Am. Chem. Soc.* **2003**, *125*, 1958.
(19) Zaera, F. *Chem. Rev.* **1995**, *95*, 2651.
(20) Bent, B. E. *Chem. Rev.* **1996**, *96*, 1361.
(21) Schulz, H. *Appl. Catal. A: General* **1999**, *186*, 3.
(22) Herrmann, W. A. *Angew. Chem., Int. Ed. Engl.* **1982**, *21*, 117.
(23) Röper, M. In *Catalysis in C_1 Chemistry*; Keim, W., Ed.; Riedel: Dordrecht, The Netherlands, 1983.
(24) Biloen, P.; Sachtler, W. M. H. *Adv. Catal.* **1981**, *30*, 165.
(25) Ge, Q.; Neurock, M.; Wright, H. A.; Srinivasan, N. *J. Phys. Chem. B* **2002**, *106*, 2826.
(26) Liu, Z. P.; Hu, P. *J. Am. Chem. Soc.* **2002**, *124*, 11568.
(27) Ciobîcă, I. M.; Kramer, G. J.; Ge, Q.; Neurock, M.; van Santen, R. A. *J. Catal.* **2002**, *212*, 136.
(28) Petersen, M. A.; Jenkins, S. J.; King, D. A. *J. Phys. Chem. B* **2004**, *108*, 5909.
(29) *CASTEP 3.9* and *4.2* academic versions; licensed under the UKCP-MSI Agreement, 1999. Payne, M. C.; Teter, M. P.; Allan, D. C.; Arias, T. A.; Joannopoulos, J. D. *Rev. Mod. Phys.* **1992**, *64*, 1045.
(30) Perdew, J. P.; Chevary, J. A.; Vosko, S. H.; Jackson, K. A.; Pederson, M. R.; Singh, D. J.; Fiolhais, C. *Phys. Rev. B* **1992**, *46*, 6671.
(31) Vanderbilt, D. *Phys. Rev. B* **1990**, *41*, 7892.
(32) Lide, D. R. (ed.), *Handbook of Chemistry and Physics*, 75th ed.; CRC Press LCC: New York, 1998.
(33) Monkhorst, H. J.; Pack, J. D. *Phys. Rev. B* **1976**, *13*, 5188.
(34) Gillan, M. J. *J. Phys.: Condens. Matter* **1989**, *1*, 689.
(35) De Vita, A.; Gillan, M. *J. Phys.: Condens. Matter* **1991**, *3*, 6225.
(36) The term agostic was coined by Brookhart and Green,[37] who used it in the context of organometallic compounds. An agostic interaction refers to situations in which a hydrogen atom is covalently bonded simultaneously to both a carbon atom and a transition-metal atom.
(37) Brookhart, M.; Green, M. L. H. *J. Organomet. Chem.* **1983**, *250*, 395.
(38) Johnson, D. F.; Weinberg, W. H. *Science* **1993**, *261*, 76.
(39) Papoian, G.; Nørskov, J. K.; Hoffmann, R. *J. Am. Chem. Soc.* **2000**, *122*, 4129.
(40) Zheng, C.; Apeloig, Y.; Hoffmann, R. *J. Am. Chem. Soc.* **1988**, *110*, 749.
(41) Hoffmann, R. *Rev. Mod. Phys.* **1988**, *60*, 601.
(42) Zhang, Y.; Yang, W. *Phys. Rev. Lett.* **1998**, *80*, 890.
(43) Anghel, A. T.; Michaelides, A.; Jenkins, S. J.; King, D. A. To be submitted for publication.
(44) Engstrom, J. R.; Tsai, W.; Weinberg, W. H. *J. Chem. Phys.* **1987**, *87*, 3104.